Applied Surface Science 615 (2023) 156318

Contents lists available at ScienceDirect

Applied Surface Science

journal homepage: www.elsevier.com/locate/apsusc

Full Length Article

Theoretical superlubricity and its friction stability of amorphous carbon film induced by simple surface graphitization

Xiaowei Li [a,b,*], Naizhou Du [a], Cunao Feng [a], Kai Chen [a], Xubing Wei [a], Dekun Zhang [a], Kwang-Ryeol Lee [c,*]

[a] School of Materials Science and Physics, China University of Mining and Technology, Xuzhou 221116, P.R. China
[b] Key Laboratory of Marine Materials and Related Technologies, Zhejiang Key Laboratory of Marine Materials and Protective Technologies, Ningbo Institute of Materials Technology and Engineering, Chinese Academy of Sciences, Ningbo 315201, P.R. China
[c] Computational Science Center, Korea Institute of Science and Technology, Seoul 136-791, Republic of Korea

ARTICLE INFO

Keywords:
Amorphous carbon
Graphitization
Superlubricity
Annealing
Friction stability

ABSTRACT

Amorphous carbon (a-C) film as one of the most promising superlubricious materials arouses much attention from technical and industrial fields. However, the superlubricious state of a-C film strongly depends on the formation of special nanostructures or components, increasing the difficulty and complexity of the preparation process. Reducing the friction coefficient of a-C film to superlubricity is still a challenge for industrial scale-up. Herein, a simple and effective approach is proposed to achieve superlubricity by in-situ formation of graphitized structure at a-C surface via fast annealing. Results reveal that the friction property closely depends on the graphitized degree of mated a-C surfaces and the friction coefficient below 0.01 or even 0.001 can be obtained for the highly graphitized system. In particular, under extreme working condition, it also demonstrates excellent stability and reliability of superlubricious behavior. This is not only mainly attributed to the decrease of spacing distance between mated graphitized structures following the high repulsive force, but also related to the tight anchoring of graphitized structure to the intrinsic a-C. In addition, compared to the widely applied surface passivation approach, the graphitization modification of a-C surface exhibits higher effectiveness in superlubricity without deteriorating the intrinsic mechanical properties of a-C film.

1. Introduction

In recent years, with the rapid development of advanced manufacturing industries such as engineering machinery, aerospace, automobile, and marine equipment, the key moving parts of mechanical systems are inevitably subject to serious friction and wear problems. These not only have a great impact on the energy dissipation, CO_2 emissions, and economic losses in the world, but also reduce the reliability and service lifetime of the system and even cause the generation of disasters [1–3]. Statistical data reveals that for the four economic sectors 23 % of the world's total energy consumption originates from tribological contacts, and due to friction and wear the total costs and CO_2 emissions globally are 250,000 million Euro and 8,120 $MtCO_2$, respectively, in 2017 [1]. Taking the passenger cars for example, 28 % of the fuel energy use goes to overcome friction in the engine, tire, and transmission with breaking friction excluded [2]. So it is required to develop the advanced surface protective technology against friction and wear for enhancing the efficiency, durability, and environmental compatibility of future mechanical systems.

So far, adding the lubricant (solid, liquid, and gas) with good anti-friction and anti-wear performance into the sliding interface has been proved to be an effective approach, which can prohibit the direct contacting of mated surfaces and thus minimize the friction coefficient and wear rate [1,2]. In particular, the presence and development of superlubricity technology, which names the friction coefficient near "zero" in an ideal state or smaller than 0.01 under industrial scale, arouses much attention in the scientific and industrial fields to alleviate the above-mentioned problems [4–7]. Among the numerous candidates, two-dimensional (2D) materials, such as graphene and MoS_2 with a single or a few layers of atoms, possess intrinsically low friction properties on their surfaces with friction coefficients below 0.01 or even 0.001, revolutionizing the field of tribology [8–11]. In addition, structural superlubricity with nearly zero friction can be endowed by the special crystalline alignment between two mated 2D materials [12–15]. For

* Corresponding authors.
E-mail addresses: lixw0826@gmail.com, xwli@cumt.edu.cn (X. Li), krlee@kist.re.kr (K.-R. Lee).

https://doi.org/10.1016/j.apsusc.2022.156318
Received 21 November 2022; Received in revised form 23 December 2022; Accepted 31 December 2022
Available online 3 January 2023
0169-4332/

example, Berman et al. [9] achieved macro-scale superlubricity by combing graphene with crystalline diamond nanoparticles and diamondlike carbon and this was because the sliding of the graphene patches around the tiny nanodiamond particles led to nanoscrolls with reduced contact area. Luo et al. [16] reported a direct measurement of sliding friction between graphene and graphene, and graphene and hexagonal boron nitride under high contact pressure, which exhibited a friction coefficient of 0.003 due to multi-asperity contact covered with randomly oriented graphene nanograins.

Although this graphene-inspired structural superlubricity holds great technical promise in actual mechanical systems, this still cannot be scaled up to macroscopic contacts for practical engineering applications because of these strict restrictions of superlubricity to macro-scale graphene structure (edge effect, surface roughness, surface defects and contamination, et al.) [12,15,17] and working conditions (humidity, substrate, load, et al.) [18,19]. These inevitable existences of wrinkles and defects for macro-scale graphene highly affect its superlubricity performance. Surprisingly, beyond graphene, amorphous carbon (a-C) film, which not only has distinguished intrinsic properties (high hardness, low friction coefficient, chemical inertness, and good wear resistance) but also can be prepared with high quality and large scale easily, can also realize the superlubricious behavior [20–24]. It has been considered as one of the most promising superlubricious candidates for industrial applications. For example, Li et al. [20,21] investigated the friction behavior of a-C composited with base oil and graphene additive and found that the ultra-low friction coefficient (<0.003) was obtained by tailoring the structure of graphene additive or passivated state a-C surface. Liu et al. [22] showed that the co-doping of Si and Al into a-C induced the formation of a self-assembled dual nanostructure constructed of cross-linking network and fullerene-like structure, which demonstrated the super-low friction coefficient (~0.001) and superior resistance. The fluorine-doped a-C film, in which the curved graphitic structures were embedded in an amorphous carbon matrix, also showed the superlubrication (friction coefficient ~ 0.01) reported by Zhang et al. [23]. Chen et al. [24] revealed that in polymer-like a-C:H:Si film the occurrence of superlubricity generally originated from a synergistic effect of phase transformation, surface passivation, and shear localization, in which the hydrogen content played a decisive role in durable superlubricity.

However, the friction coefficient of a-C film is normally limited to a range larger than 0.01 [25,26]. Previous studies [20–24,27] also conveyed that the occurrence and maintenance of the superlubricious state of a-C film highly depend on the formation of special nanostructures or components at the friction interface. This will increase the difficulty and complexity of the preparation process, which is inconducive to the industrial scale-up. Hence, reducing the friction coefficient of a-C film below 0.01 or even 0.001 is still a challenge in practice. Especially, to promote the superlubricious industrialization of a-C film, a simple and effective approach is indispensable. Based on the two popular low-friction mechanisms of a-C film [27–29], graphitizing or passivating the a-C surface is suggested to address the problems. Among them, hydrogen-induced passivation of a-C surface, which can effectively eliminate the negative effect of interfacial dangling bonds, has been widely investigated and adopted to arrive superlubricity [5,24,30], but under the extreme condition such as high load, the friction coefficient displays an unexpected increase obviously [31]. Furthermore, excessive H content also deteriorates the intrinsic mechanical property of a-C film [25,26]. While similar to Luo's studies [16,32], introducing graphene or other 2D materials into the friction interface of a-C films is also an important way for superlubricity according to the graphitization mechanism without deteriorating the intrinsic structure of a-C film. However, our previous study revealed that the stable existence and positive function of extra graphene structure are highly sensitive to the interfacial dangling bonds, size and shape of graphene [29], leading to the higher cost and un-uniform size control at friction interface.

In order to solve the problems, in the present work, a robust strategy is proposed to achieve superlubricity by in-situ formation of the graphitized structure via surface annealing. This can eliminate the uncontrollability and complexity of the interaction between direct-added graphene and a-C surface. Optimized temperature for fast surface annealing was suggested. During the friction process, the surface graphitized layer was chemically anchored to the intrinsic a-C structure to improve the stability, while the friction behavior occurred at the mated graphitized structure by weak intermolecular interaction to reduce the friction resistance. The system with a higher-quality graphitized structure exhibited superior superlubricity and friction stability even under extreme working conditions.

2. Computational details

All reactive molecular dynamics (RMD) calculations, including the graphitization of pre-deposited a-C surface by fast annealing process and the friction simulation, were employed by Large-scale Atomic/Molecular Massively Parallel Simulator (LAMMPS) code [33]. Reactive force field (ReaxFF) interatomic potential [34–36] was used to describe the C—C interaction and the transformation of hybridized structure, which uses the bond order concept to consider the instantaneous interaction between the atoms and thus allows for the formation and dissociation of the covalent bond and the chemical reactions in complicated carbon-based systems with high accuracy as compared to the quantum calculations. The reliability of the used force field to our present calculations has been validated adequately by our previous calculations [21,29,37]. In addition, it was also confirmed by the comparative results of the graphitized transformation of a-C surface using AIREBO [38] and ReaxFF potentials, respectively, as shown in Fig. S1 of Supplementary Data.

2.1. Fabrication of the graphitized surface of a-C film

The initial a-C structure with a size of 42.88 × 40.358 × 36.5 $Å^3$ was set as the substrate, which was composed of 6877 carbon atoms and had the sp^3-C fraction of 24 at.%, sp^2-C fraction of 72 at.%, and density of 2.7 g/cm^3. It was deposited using atom-by-atom method and the detailed deposition process was described elsewhere [39]. In order to fabricate the graphitized surface of a-C film, the annealing procedure was performed by a canonical ensemble employing the Nose-Hoover thermostat [40] with a damping constant of 100 fs, as shown in Fig. 1a. During the annealing process, the a-C surface with the thickness of 12.5 Å was first relaxed at each defined temperature for 1250 ps, which ranged from 300 to 3000 K in order achieve the different surface graphitized structures; then, the system was cooled down to 300 K with a cooling rate of 2.4 × 10^{14} K/s. Finally, the a-C films with different graphitized surfaces were obtained after the additional relaxation at 300 K for 25 ps. In the following study, the films with different surface graphitized degrees were named as a-C@*T* separately according to the annealing temperature, *T*, for each case.

2.2. Friction simulation

For the friction model, it was also composed of self-mated a-C films with different graphitized surfaces. Similar to the previous studies [37,41], a three-layer assumption model was applied to each system in Fig. 1b, including the rigid layer for simulating the semi-infinite system, the thermostatic layer being maintained at 300 K through the micro-canonical ensemble with a Berendsen thermostat [42], and the free layer consisted of the remnant atoms for modeling the evolution of tribo-induced interfacial structure. The time step was 0.25 fs. Periodic boundary condition was imposed along both the *x*- and *y*-directions.

During the friction process, a three-step process was adopted: (i) geometric optimization at 300 K for 2.5 ps; (ii) loading process to achieve the specified value of contact pressure (5 ~ 50 GPa) during 25 ps; (iii) sliding process with fixed contact pressure and sliding velocity (10

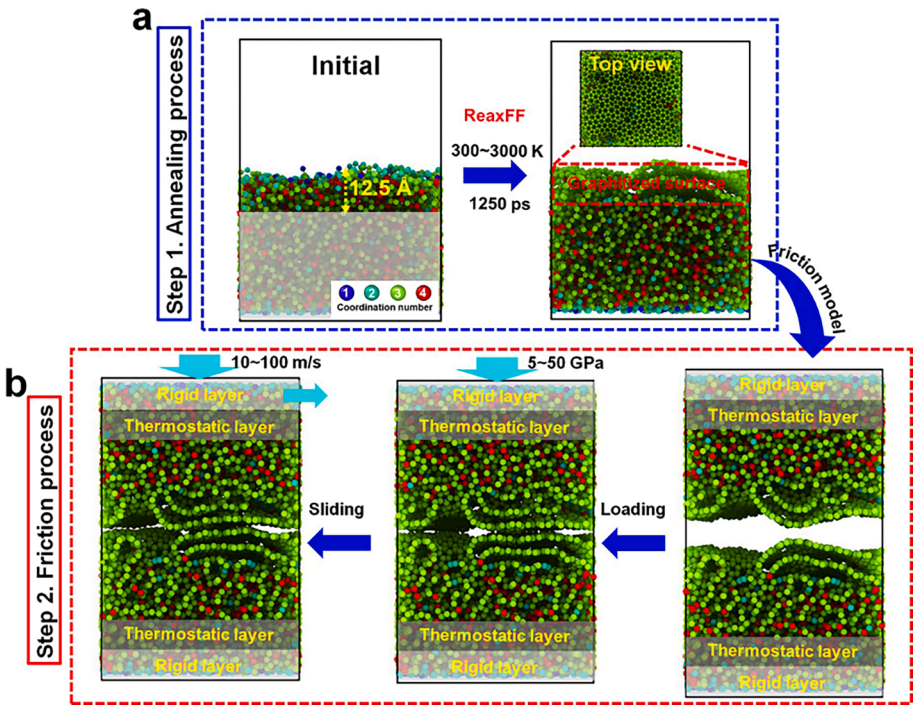

Fig. 1. Models of graphitized a-C surface fabricated by annealing and the self-mated friction systems.

~ 100 m/s) along the *x*-direction for 1250 ps. In particular, extreme working conditions, such as high contact pressure of 50 GPa and high sliding velocity of 100 m/s, were also considered to test the friction stability of the system. Although these contact pressure and sliding velocity values were much higher than those in the experiment, our [21,29,37,43] and previous studies [41,44,45] have already confirmed that they were appropriate to examine the friction behavior from an atomic scale. After the friction process, the forces from the × and *z* directions of the rigid layer of the bottom a-C substrate were counted as friction force, *f*, and normal force, *W*, respectively, for each case; the real contact area, *A*, and shearing strength, *S*, were calculated according to Hertzian theory:

$$A = \frac{W}{\sigma} \tag{1}$$

$$\mu = \frac{f}{W} = \frac{S \times A}{W} = \frac{S}{\sigma} \tag{2}$$

where μ was the friction coefficient and σ was Hertzian contact pressure, which was 5, 30, and 50 GPa, respectively, in this work.

3. Results and discussion

3.1. Structural analysis of graphitized a-C

During the annealing process of a-C surface at different

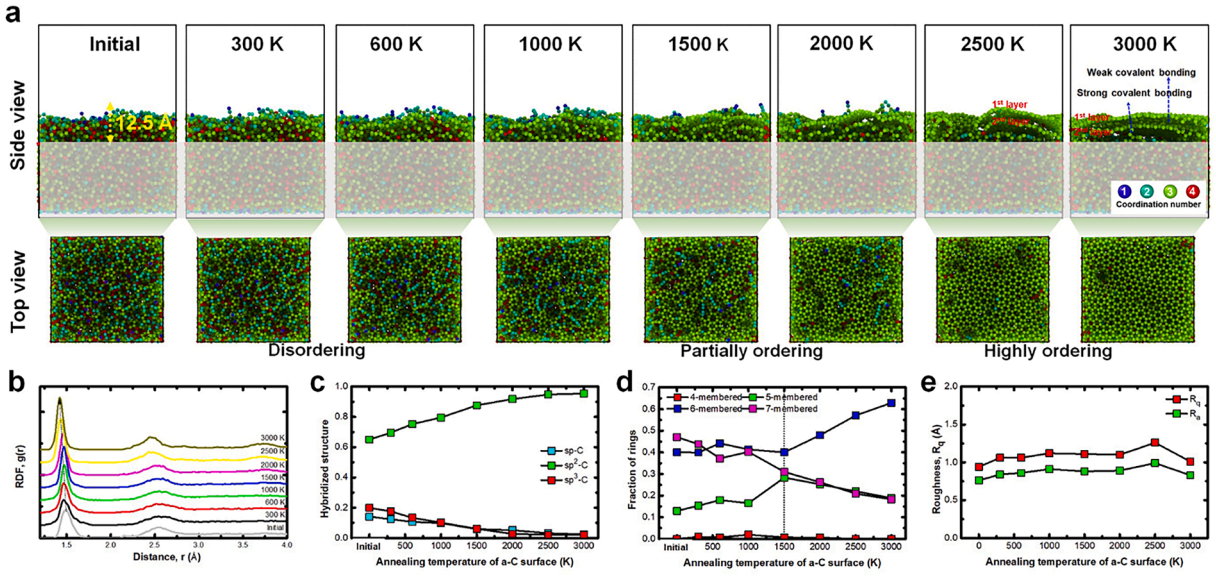

Fig. 2. Final morphologies after annealing process and structural transformation as a function of annealing temperature of a-C surface with thickness of 12.5 Å: (a) morphologies, (b) RDF spectra, (c) hybridized structure, (d) fraction of rings, and (e) roughness.

temperatures, the structural transformation is evaluated first, as shown in Fig. S2 of Supplementary Data. It can be seen that for each case, the fraction of the sp^2-C hybridized structure increases quickly and then become stable during the annealing time of 1250 ps, while the fraction of the 6-membered ring shows an obvious increase only under 2500 and 3000 K. After the annealing process of a-C surface with thickness of 12.5 Å, Fig. 2 gives the corresponding final morphologies and structural transformation as a function annealing temperature, including radial distribution function (RDF) curve, roughness, hybridization, and the fraction of rings. With the annealing temperature ranged from 300 to 3000 K, the surface morphology of a-C changes from the amorphous and disordering state to a highly ordering state (Fig. 2a and Fig. S3 of Supplementary Data). Even the a-C surface with obvious double layer structure is observed at both a-C@2500 and a-C@3000 K, in which the 2nd layer interacts with the bottom a-C structure with strong chemical bonding, while there are still a few chemical bonds existed between the 1st and 2nd layers. This is also confirmed by the RDF spectra (Fig. 2b), in which the width of the 1st and 2nd peaks decreases while their strength increases. In addition, it should be mentioned that during the annealing process, the generation of different layer numbers of graphitized structure in Fig. 2 is sensitive to the annealing parameters, such as temperature and time.

For the hybridized structure of annealed a-C surface in Fig. 2c, the sp^2-C fraction with annealing temperature increases quickly and then becomes stable at 3000 K which is accompanied by the reduction of sp^3-C and sp-C fractions according to the *P-T* diagram [28]. Moreover, the analysis of ring structure (Fig. 2d) of annealed a-C surface reveals that as the annealing temperature increases from 300 to 1500 K, the fraction of the 6-membered ring has a slight change, but the 7-membered ring transforms into the 5-membered ring. With further increasing the temperature to 2000, 2500, and 3000 K, the fraction of 6-membered rings rises quickly with the reduction of both 5-membered and 7-membered rings. In addition, the roughness of a-C is also evaluated (Fig. S4 of Supplementary Data), which has a slight change for each case (Fig. 2e). From the results in Fig. 2, it suggests that the high-temperature and short-time annealing treatment can achieve the graphitized structure of a-C surface with high quality while without deteriorating the intrinsic structure of a-C film, different with the hydrogenated modification of a-C [25,26]. The optimized values of annealing parameters, such as temperature 3000 K and time 1250 ps, are suggested, which can be realized experimentally by femtosecond laser irradiation.

3.2. Friction dependence on the graphitized degree of a-C surface (5 GPa)

3.2.1. Friction property induced by surface graphitization

Fig. 3a gives the friction curve during the sliding process for each case. It shows that for the a-C@300 K, there is an obvious running-in process which takes about 500 ps to reach the stable-friction stage. However, with increasing the annealing temperature, especially a-C@2500 and a-C@3000 K, the surface graphitized degree is enhanced and thus significantly reduces the time for the running-in process.

The values during the last 200 ps of the friction curve are adopted to calculate the average friction force and normal force values for each case, as illustrated in Fig. 3b. The normal force is similar for each case which decreases first and then increases slightly, being in consistence with the real contact area (Fig. S5 of Supplementary Data) at the interface according to Eq. (1). While the change of real contact area is closely related with not only the surface roughness of a-C film (Fig. 2e) but also the formation of large-scale graphitized structure (Fig. 2a). For the friction force value, it has slight change as annealing temperature changes from 300 to 1000 K, but with the further increase of annealing temperature, the friction force drops drastically and then become stable at 2500 and 3000 K.

The friction coefficient is calculated for each case according to Eq. (2), as shown in Fig. 3c, which is similar to the change of friction force with annealing temperature. For a-C film annealed at the temperature smaller than 1000 K, the system exhibits a high value of friction coefficient, which is consistent with the initial case. However, it should be noted that these values are much higher than experimental ones because the a-C surface used in present RMD simulations has no any surface contamination or passivation as that in the experiment [31,37,43], inducing the strong adhesive interaction of mated materials. However, for the a-C@3000 K system, the minimal value of friction coefficient, 0.016, is obtained, which is reduced by 99.8 % compared to the initial case and close to the superlubricious state [4–7]. In addition, according to Eq. (2), the calculated shearing strength with annealing temperature (Fig. S5 of Supplementary Data) is also in accordance to the friction coefficient (Fig. 3c). The improvement of a-C surface graphitization also lowers the temperature rise at the friction interface (Fig. S5 of Supplementary Data), which is mainly dominated by the friction force (Fig. 3b) in the present work according to previous reports [37,46].

3.2.2. Transformation of interfacial structure

In order to clarify the friction dependence on the graphitized degree of the a-C surface in Fig. 3, the transformation of the interfacial structure needs to be explored. Before that, the interfacial width of the friction system should be identified first. Fig. 4 shows the distributions of C atoms from mated a-C films with sliding time for mated initial a-C and a-C@3000 K systems, respectively. For the initial a-C system (Fig. 4a), there is an obvious transformation of interfacial structure with sliding time, suggesting the significant interaction of mated a-C surfaces, similar to previous works [29,37]. However, with the increase of the graphitized degree of a-C surface, this weakens the change of friction interface. Taking the a-C@3000 K system for example, the interfacial structure almost has no change with sliding time, as provided in Fig. 4b.

Compared to the initial structure, the film structure (<24 Å) has no change during the sliding process, so the structure of film with thickness above 24 Å is adopted for quantifying the interfacial structure for each case. Hence, the different evolutions of friction interface with sliding time in Fig. 4, which are induced by different graphitized surfaces of a-C

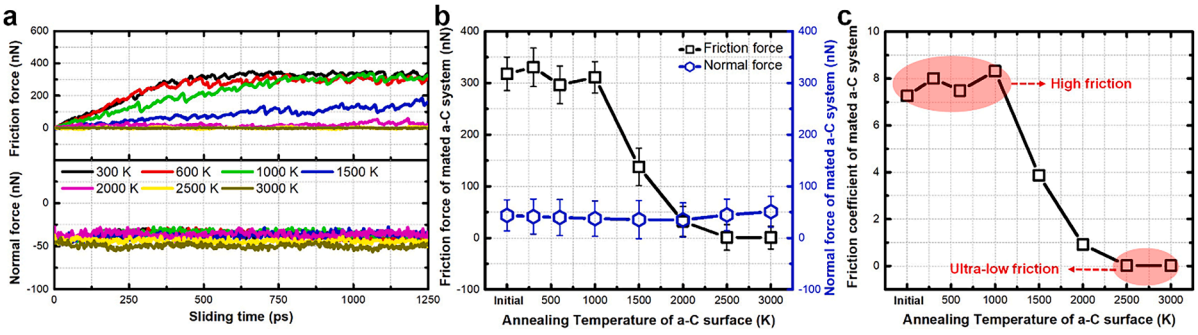

Fig. 3. Friction property induced by surface graphitization for each case: (a) friction curves, (b) average friction force and normal force values as a function of annealing temperature, and (c) friction coefficient as a function of annealing temperature.

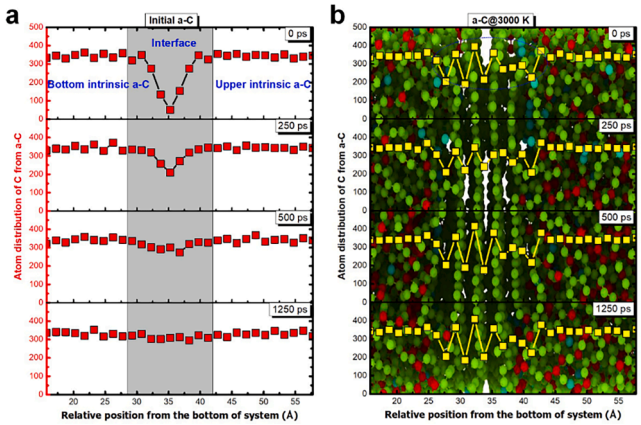

Fig. 4. Distributions of C atoms from a-C films with sliding time for mated (a) initial a-C and (b) a-C@3000 K systems, respectively.

films, are also confirmed by the following analysis of interfacial structure including hybridized (sp^3-C, sp^2-C, and sp-C) and ring (5-, 6-, and 7-membered rings) structures, as shown in Fig. S6 of Supplementary Data. Moreover, Fig. S6 of Supplementary Data also reveals that for these systems with weak graphitized surfaces, the sp^3-C fraction decreases first and then becomes stable during the sliding process from 0 to 1250 ps, which is contrary to the change of the sp^2-C fraction, as consistent with previous results [29,47]. This indicates the shearing-induced transformation of sp^3-C to sp^2-C [28], and it is also accompanied by the increased sp-C fraction due to the shearing-induced breaking of the C—C bond. For the highly graphitized surface of a-C film, the lack of the above-mentioned structural transformation implies weak or no chemical interaction of mated a-C surfaces.

Fig. 5 shows the calculated results of hybridized and ring structures of friction interface as a function of annealing temperature after the sliding process, in which those before the sliding process are also given for comparison. First, the above-mentioned data in Fig. 2 reveals that as the annealing temperature increases from 300 to 3000 K, the graphitized degree and its ordering of a-C surface is highly improved. This highly affects the structure of the friction interface after the sliding process, leading to the plots in Fig. 5 being divided into three regions.

Region I: as increasing the annealing temperature from 0 to 1000 K, the a-C surface has no or weak graphitized degree with disordering distribution, and both the sp^3-C and sp-C fractions and 7-membered ring fraction before the sliding process decrease while the sp^2-C and 5-membered ring fractions increase. However, after the sliding process, due to the strongly cold-welding between mated a-C surfaces, shearing induces the reduction of sp^3-C and 7-membered ring fractions, which transforms to sp^2-C, sp-C, and 5-membered ring, respectively (Fig. 5). This is in agreement with previous studies [28,47]. So after the sliding process, the cases including a-C@300 K, a-C@600 K, and a-C@1000 K exhibit similar interfacial structure as the initial case without surface annealing. This contributes to the change in friction coefficient in Fig. 3.

Region II: In this region, the annealed a-C film has a graphitized surface with partially ordering following the decrease of sp^3-C, sp-C, 5-membered and 7-membered ring structures, but both the sp^2-C and 6-membered ring fractions increase, being related with the quality improvement of the graphitized structure. Compared to that before the sliding process, the evolution of interfacial structure after the sliding process shows similar dependence on the annealing temperature. Nevertheless, only the obvious transformation of sp^2-C-to-sp-C is observed before and after friction processes (Fig. 5) due to the shearing-induced dissociation of sp^2-C structures. Compared to the serious change in region I, this minor change attributes to the quality of surface graphitized structure and reduction of dangling bonds, as will be discussed later.

Region III: the a-C surface is highly graphitized with ordering distribution. With increasing the annealing temperature, the hybridized structure has no change, but the 5-membered and 7-membered rings tend to be transformed to 6-membered rings obviously for polishing the graphitized quality. In particular, the interfacial structure including hybridization and rings after the sliding process almost has no change by comparing with that before the sliding process, as shown in Fig. 5, further confirming the absence of chemical cross-linking during the friction process. Therefore, from the results in Fig. 5, it can be deduced that the increase of the graphitized degree of the a-C surface will weaken the shearing and cross-linking interaction between mated a-C surfaces, and thus affects the transformation of the interfacial structure during the sliding process.

Furthermore, the sp^2-C and sp-C at the friction interface may contribute to the dangling bonds which normally dominate the friction property of mated a-C films [31,47]. Fig. 6 further gives the statistical analysis of interfacial dangling bonds for each case before and after sliding processes separately. It can be seen that before the sliding process, with the increase of surface graphitized degree, the number of dangling bonds shows a monotonous and fast decrease first in region I, then drops gradually in regions II, and finally becomes stable in region III. It has similar behavior to that of the sp^3-C fraction in Fig. 5. However, after the sliding process, the change of the number of dangling bonds

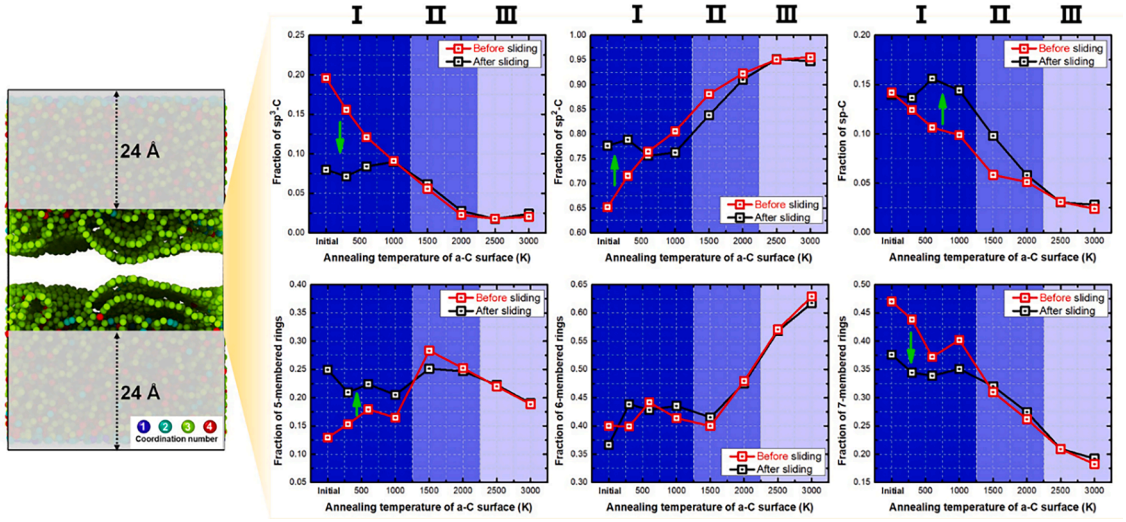

Fig. 5. Hybridized and ring structures of friction interfaces as a function of annealing temperature before and after sliding processes separately.

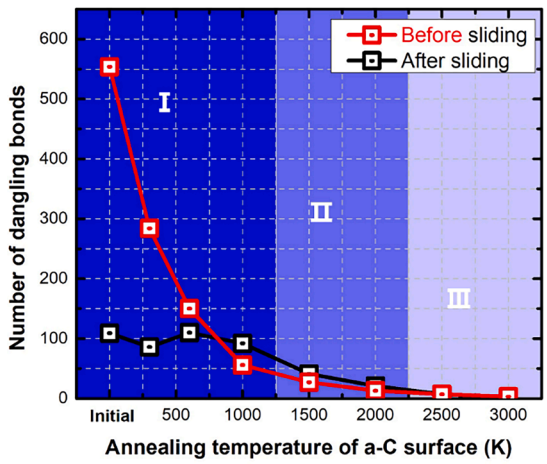

Fig. 6. Statistical analysis of interfacial dangling bonds for each case before and after sliding processes separately.

with the surface graphitized degree is also similar to that before the sliding process except for the region I. These systems in region I show the close values of the number of dangling bonds, but these values are still much higher than those in regions II and III, accounting for the high friction coefficient in Fig. 3. Furthermore, compared to that before the sliding process, there is a drastic reduction of the number of dangling bonds observed in region I, originating from the friction-induced structural transformation and interfacial cross-linking. But in region II, a slight increase in the number of dangling bonds after the friction process is present due to the shearing effect and the defects of the graphitized structure. In addition, note that the change of dangling bonds with annealing temperature agrees well with the friction coefficient in Fig. 3. The above-mentioned change of interfacial structure can be also confirmed by Fig. S7 of Supplementary Data and Supplementary Movies S1 ~ S7.

3.2.3. *Friction mechanism under low contact pressure of 5 GPa*

According to the analysis of interfacial structure, the friction behavior under the contact pressure of 5 GPa can be explained for each case. First, for the systems with no or weak graphitized surface, such as those in region I of Fig. 5, surface annealing causes the increase of sp^2-C fraction but with disordering distribution (Fig. 2 and Fig. S3 of Supplementary Data). In addition, they still have a high fraction of dangling bonds (Fig. 6). They reconstruct the friction interface during the sliding process by the strongly adhesive interaction between unsaturated hybridized structures of mated a-C surfaces, as confirmed by Fig. S7 of Supplementary Data. So these systems, such as a-C@300, a-C@600, and a-C@1000 K, give similar interfacial structures (Figs. 5 and 6) following the high friction coefficient (Fig. 3).

For the systems in region II, such as a-C@1500 and a-C@2000 K, increasing the annealing temperature improves the quality of the graphitized structure of the a-C surface moderately and also reduces the fraction of sp-C hybridization (Fig. 6). Although some graphitized structures are formed (Fig. 2), they have small size and are also randomly distributed in amorphous carbon networks. On the one hand, due to the decrease of interfacial dangling bonds, it weakens the chemically adhesive interaction of mated a-C surfaces significantly during the friction process, contributing to the decrease of tensile stress at the friction interface (Fig. S8 of Supplementary Data and Fig. 7a). On the other hand, some graphitized structures are contacted with each other during friction process by intermolecular interaction, but the existed sp-C dangling bonds still result in the chemical cross-linking between mated a-C surfaces to support the applied normal load, leading to the physically contacted graphitized structures with large spacing distance, such as 4.0 Å in a-C@2000 K system (Fig. 7a). This corresponds to the small repulsive or even attractive interaction, which plays a limited role in the friction reduction (Fig. 3), while it is mainly dominated by the decrease of interfacial dangling bonds.

For the systems in region III, such as a-C@2500 K and a-C@3000 K, the graphitized structure with high quality (large size, high ordering) is generated at the a-C surface and the sp-C hybridization is absent (Fig. 2). Hence, there almost has no dangling bonds at the friction interface (Fig. 6), suggesting the absence of adhesive interaction between mated a-C surfaces. Fig. 7b shows that the interfacial stress changes from tensile to compressive state due to the transformation of the binding state between mated a-C surfaces from covalent to weak intermolecular interaction. In addition, because the graphited structures at mated a-C surfaces are highly contacted during the friction process (Fig. 7b), the friction behavior is also dominated by the strength of intermolecular

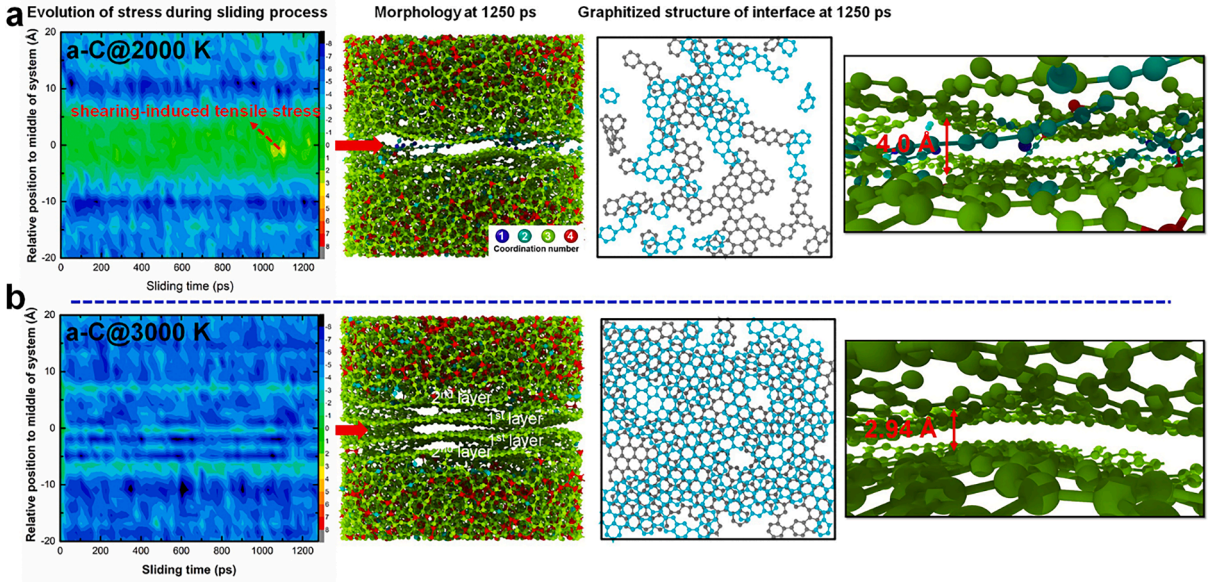

Fig. 7. Interfacial structure and property, including the mapping of stress evolution during the sliding process, morphologies at 1250 ps, the graphitized structure of interface at 1250 ps (only 6-membered ring is considered), and spacing distance between contacted graphitized structures in (a) a-C@2000 and a-C@3000 K systems, respectively.

interaction between graphitized structures and roughness surface. For the a-C@3000 K system, the spacing distance of interacted graphitic structures is only 2.94 Å, smaller than the standard value (~3.40 Å) for graphene [48], suggesting a high repulsive force. So these result in the ultra-low friction coefficient in Fig. 3 following the significant increase of real contact area (Fig. S5 of Supplementary Data). The schematic diagram for the friction mechanism under different graphitized degrees of a-C surfaces is given in Fig. 8.

3.3. Friction stability of surface graphitized a-C under extreme working conditions

To evaluate the stability of the mated a-C friction system and its dependence on the graphitized degree of the a-C surface, extreme working conditions, including high contact pressure (30 and 50 GPa) and sliding velocity (100 m/s), are applied, mainly focusing on the systems with moderate and highly graphitized surfaces (a-C@1500, a-C@2000, a-C@2500, and a-C@3000 K). Fig. 9a gives the corresponding friction coefficient for each case. Results show that for these no and weak graphitized cases (such as a-C@300 K), as the contact pressure and sliding velocity increase to the values of 50 GPa and 100 m/s separately, the friction coefficient displays a significant reduction, attributing to the passivation of friction interface, as confirmed by previous experimental and simulation works [46,47].

For the systems with the moderated graphitized surface, taking the a-C@1500 K system for example, it can be seen that compared to the result in Fig. 3, as only the sliding velocity changes to 100 m/s from 10 m/s with the same contact pressure of 5 GPa, the friction coefficient increases (Fig. 9a). This is because the increase of velocity is normally followed by the temperature rise of friction interface (Fig. 9b) [37,46], aggravating the chemical bonding of both dangling bonds and small graphitized structures at mated a-C surfaces (Figs. 2 and 6). On the one hand, this strongly interfacial interaction causes the partial dissociation of small graphitized structures (Fig. S3 of Supplementary Data); on the other hand, it brings high shearing resistance. However, due to the relatively low contact pressure (5 GPa), the transformation of the interfacial structure only occurs at the shallow surface of a-C film, which can be confirmed by the slight change of real contact area in Fig. 9c, without enough interfacial passivation, explaining the increased friction coefficient (Fig. 9a). With further increasing the contact pressure to 50 GPa, the friction coefficient also tends to be the level as a-C@300 K, which is also due to the shearing-induced reconstruction of friction interface, including interfacial passivation by sp^2-C-to-sp^3-C and sp-C-to-sp^3-C transformation [28,46] and the complete dissociation of the small graphitized structures. This can be validated by the change of interfacial morphologies after the friction process under different working conditions, as illustrated in Fig. 10 and Supplementary Movie S8. Similar behavior is also observed for the a-C@2000 K system.

For the a-C@2500 K system with a high-quality graphitized structure of a-C surface, when the sliding velocity and contact pressure are 100 m/s and 5 GPa, respectively, the friction coefficient drops to 0.013 from 0.022 (5 GPa-10 m/s) (Fig. 9a), which attributes the decrease of spacing distance between contacted graphitized structures, leading to the transformation of their interactive force from attractive to repulsive state (Fig. 11 and Fig. S9 of Supplementary Data) following ultra-low friction force. So there is no increase in interfacial temperature (Fig. 9b) and real contact area (Fig. 9c). With the contact pressure further increased to 30 GPa, there is cross-linking observed between mated a-C surfaces (Fig. 11), which will suppress the sliding process. However, the applied load further reduces the spacing distance between mated graphitized structures (2.29 Å) (Fig. 11) following the increase of real contact area (Fig. 9c). This suggests the enhancement of their repulsive interaction, which can also support the applied normal load. The competition of the above-mentioned two factors increases shearing strength much slower than that of contact pressure, so it still exhibits the ultra-low friction coefficient (0.014) (Fig. 9a). While with the contact pressure of 50 GPa applied, it aggravates the chemical cross-linking and also brings the high-temperature rise of the interface (Fig. 9b), thus leading to the complete dissociation of graphitized structure (Fig. 11 and Supplementary Movie S9) and the serious increase of shearing strength. This can account for the high friction coefficient but is also close to the cases without surface annealing.

Moreover, for the a-C@3000 K system, it has the best quality of graphitized surface than other systems. Fig. 9a reveals that it exhibits the best friction stability and reliability under any extreme working conditions. Under 5 GPa and 100 m/s, the friction coefficient is only 0.0026, achieving superlubricious state. With increasing the contact pressure from 5 GPa to 50 GPa, the friction coefficient further decreases to be superlubricious value of 0.001. Although the increased contact pressure brings an increase in the real contact area, there is no chemical bonding existed between mated a-C surfaces due to the absence of dangling bonds (Fig. 6) and there is also no structural evolution of mated graphitized surfaces, as confirmed by Fig. 12 and Supplementary Movie S10. However, due to the increased contact pressure, it induces the improvement of the quality of interfacial graphitized structures, which can be confirmed by the interfacial morphologies and the intensity and width of peaks in Fig. 12. This is followed by the gradual reduction of spacing distance between mated graphitized structures from 2.94 to 2.20 Å (Fig. 12), increasing the repulsive forces of friction interface and thus promoting the shearing behavior, which plays a key role for the superlubricious state. In addition, different with the extra-added graphene [17,29,32], in the present study, these mated graphitized structures at the friction interface are tightly anchored to the intrinsic a-C structures, respectively, without obvious migration and diffusion, which also contributes to the friction stability under extreme condition.

3.4. Comparison of anti-friction effectiveness induced by graphitization and hydrogenated passivation of a-C surface

In order to examine the anti-friction effectiveness between graphitization and hydrogenated passivation of a-C surface, Fig. 13 shows the comparative results of friction coefficient under low and high contact pressure, respectively. It can be seen that when the contact pressure is 5 GPa (Fig. 13a), with increasing the graphitized or passivated degree of a-

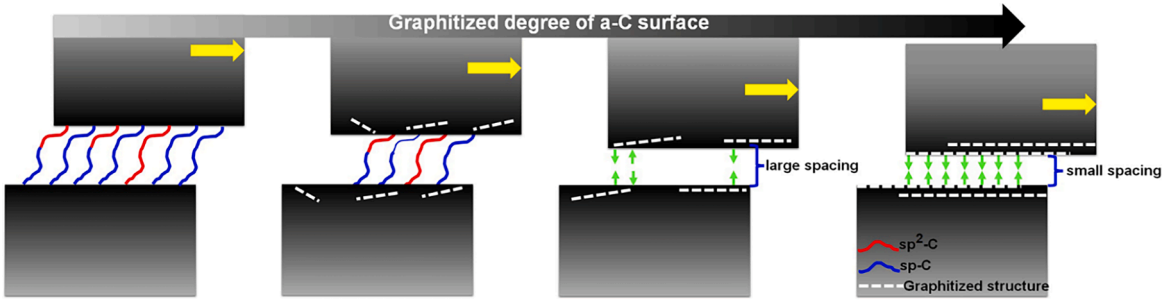

Fig. 8. Schematic diagram for friction mechanism under different graphitized degrees of a-C surfaces.

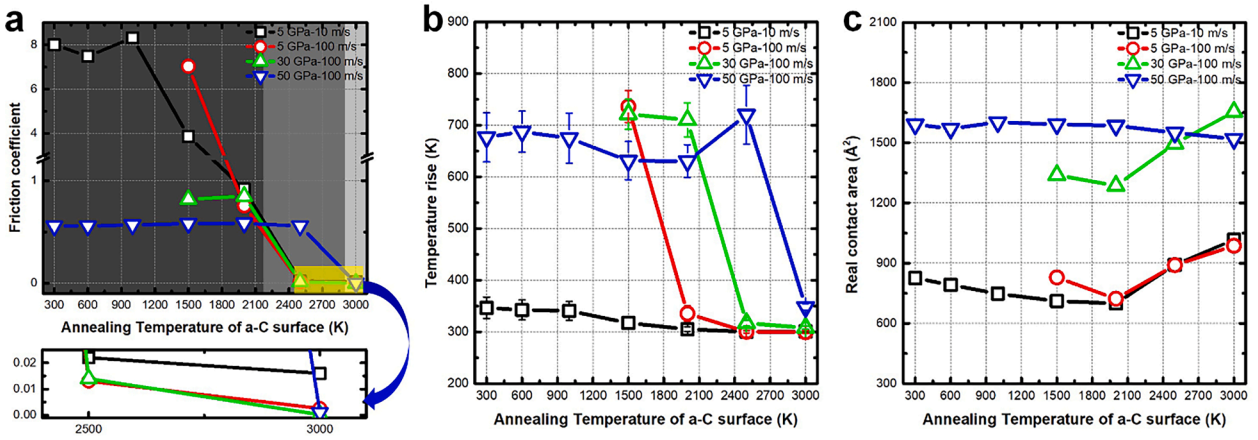

Fig. 9. Friction results of systems with different graphitized degrees under extreme working conditions, including high contact pressure (30 and 50 GPa) and sliding velocity (100 m/s): (a) friction coefficient, (b) temperature rise of friction interface, and (c) real contact area of friction interface.

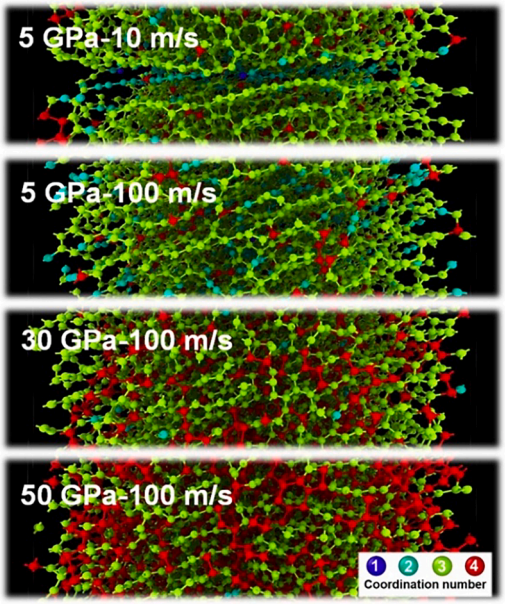

Fig. 10. Interfacial morphologies of a-C@1500 K system after friction process under different working conditions.

C surface, the decreasing speed in friction coefficient is fast first and then slow. However, compared to the case with enough surface passivation, the system with a highly graphitized surface exhibits a lower friction coefficient, due to the weak intermolecular interaction of interacted graphitized structures (Fig. 7), as reported by a previous study [29]. Although for the surface passivation approach, especially the full hydrogenation of a-C structure [5,24,30], the friction coefficient can be further decreased with surface H content (inset of Fig. 13a), this also unexpectedly deteriorates the intrinsic mechanical property of a-C film and anti-wear performance [25,26] and is also accompanied by the increased friction coefficient with contact pressure [31].

However, under the extreme working condition (contact pressure 50 GPa), the friction coefficient with passivation degree of a-C surface decreases gradually [31], while weak or moderate graphitization of a-C surface cannot play a positive role in reducing the friction coefficient, agreeing well with previous works [20,29]. But once the a-C surface has a graphitized structure with high quality, the friction coefficient drops significantly, reaching the superlubricious state (Fig. 13b), which cannot be obtained through H-induced surface passivation. Most importantly, the friction coefficient further decreases with the increase of contact pressure (Fig. 9a), being contrary to the hydrogenation case. In addition, because only the a-C surface is graphitized without deteriorating the intrinsic structure of a-C, it still remains the excellent mechanical properties. Hence, compared to the surface passivation approach, the graphitization of a-C surface exhibits higher effectiveness in superlubricity, which is also easy to be realized on a macroscale by femtosecond laser irradiation for engineering applications, as confirmed by Liu's study [49].

4. Conclusions

In the present work, we fabricated self-mated a-C friction systems, in which the a-C surface was graphitized by fast annealing treatment under different temperatures. By the systematical analysis of friction property and interfacial structure through RMD simulation, results revealed that:

- The friction behavior was strongly dependent on the graphitized degree of the a-C surface. Under the contact pressure of 5 GPa, for the system with no and weak graphitized a-C surface, the friction coefficient was high, similar to the initial case, while with further improving the graphitized degree of a-C surface, the friction coefficient decreased quickly, and then become stable for highly graphitized systems, close to superlubricious state.
- In particular, under extreme working conditions, for systems with a weak or moderate graphitized surface, although high normal force promoted the interfacial passivation, it also aggravated the chemical cross-linking and brings the high-temperature rise of the interface, leading to the dissociation of graphitized structure and the serious increase of shearing strength. On the contrary, for the system with high-quality graphitized surfaces, such as a-C@3000 K, it achieved superlubricious behavior with friction coefficient below 0.01 or even 0.001. In particular, it exhibited the superlubricious stability and reliability under different working conditions. Interfacial analysis clarified that the superlubricious mechanism not only attributed to the decrease of spacing distance between contacted graphitized structures following the high repulsive force, but also the tight anchoring of graphitized structure to the intrinsic a-C structure.
- Furthermore, compared with the results induced by enough passivation of a-C surface, the system with a highly graphitized surface had a lower friction coefficient due to the weak intermolecular interaction of contacted graphitized structures. Especially under extreme working conditions, graphitizing the a-C surface could realize the superlubricious state, which was unable to be obtained through H-induced surface passivation, indicating the effectiveness in superlubricity by surface graphitization of a-C film.

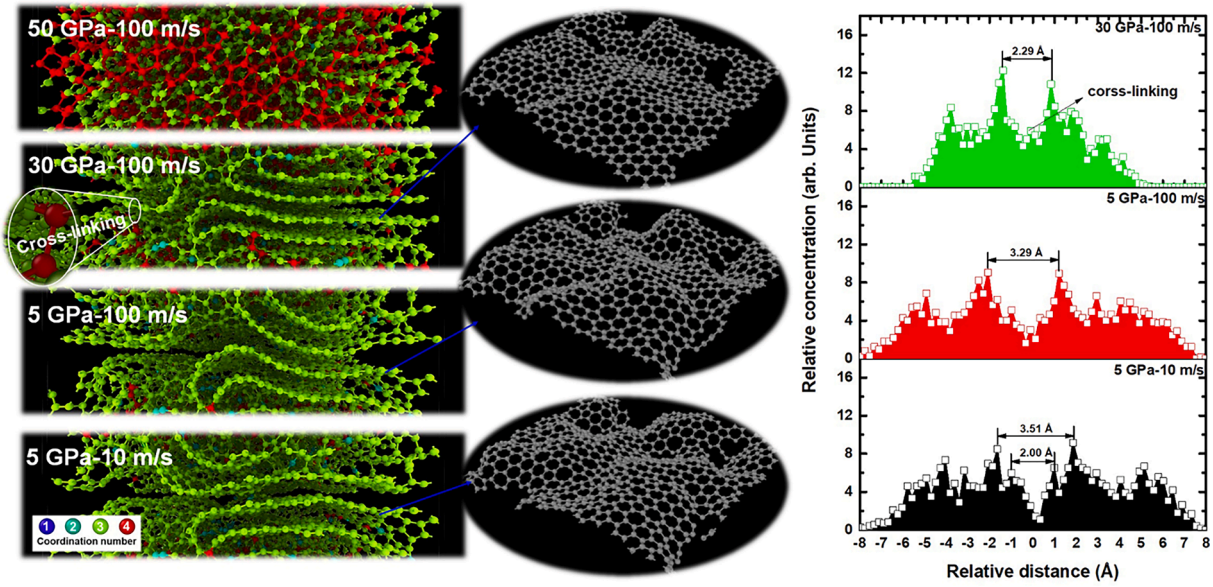

Fig. 11. Interfacial morphologies, partial graphitized structure, and relative concentration of only mated graphitized structures of a-C@2500 K system after friction process under different working conditions.

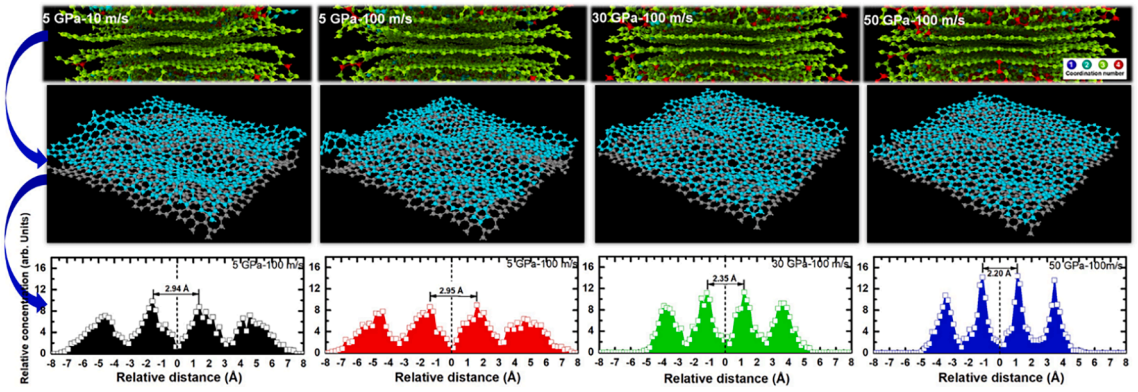

Fig. 12. Interfacial morphologies, mated graphitized structures, and its relative concentration of a-C@30000 K system after friction process under different working conditions.

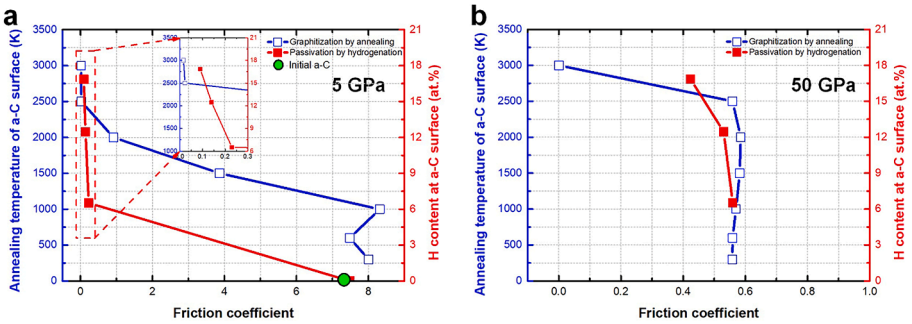

Fig. 13. Comparative results of friction coefficient induced by surface graphitization and passivation of a-C film under the contact pressures of (a) 5 GPa and (b) 50 GPa, respectively.

- These present results disclose the relation of friction property with the graphitized degree of a-C surface and the fundamentally superlubricious mechanism which is not accessible for an experimental approach and most importantly develop the fast and facile method for fabricating the superlubricious a-C film for industrial scale-up and applications.

CRediT authorship contribution statement

Xiaowei Li: Conceptualization, Data curation, Funding acquisition, Formal analysis, Methodology, Investigation, Resources, Supervision, Writing – original draft, Writing – review & editing. **Naizhou Du:** Data curation, Formal analysis, Methodology, Investigation, Visualization,

Writing – original draft. **Cunao Feng:** Formal analysis, Methodology, Investigation, Writing – original draft. **Kai Chen:** Formal analysis, Methodology, Investigation, Writing – original draft. **Xubing Wei:** Formal analysis, Methodology, Investigation, Writing – original draft. **Dekun Zhang:** Conceptualization, Writing – review & editing, Resources. **Kwang-Ryeol Lee:** Conceptualization, Data curation, Investigation, Resources, Supervision, Writing – review & editing.

Declaration of Competing Interest

The authors declare that they have no known competing financial interests or personal relationships that could have appeared to influence the work reported in this paper.

Data availability

Data will be made available on request.

Acknowledgments

This research was supported by the National Natural Science Foundation of China (No.52175204), Basic Research Program of Xuzhou (No. KC21041), Material Science and Engineering Discipline Guidance Fund of China University of Mining and Technology (No. CUMTMS202211), and Graduate Innovation Program of China University of Mining and Technology (No. 2022WLJCRCZL281). Special thanks to the Analysis and Testing Center of China University of Mining and Technology for their help with the calculation platform.

Appendix A. Supplementary material

Supplementary data to this article can be found online at https://doi.org/10.1016/j.apsusc.2022.156318.

References

[1] K. Holmberg, A. Erdemir, Influence of tribology on global energy consumption, costs and emissions, Friction 5 (3) (2017) 263–284.
[2] K. Holmberg, P. Andersson, A. Erdemir, Global energy consumption due to friction in passenger cars, Tribol. Int. 47 (2012) 221–234.
[3] K. Holmberg, P. Kivikytö-Reponen, P. Härkisaari, K. Valtonen, A. Erdemir, Global energy consumption due to friction and wear in the mining industry, Tribol. Int. 115 (2017) 116–139.
[4] M. Hirano, K. Shinjo, R. Kaneko, Y. Murata, Anisotropy of frictional forces in muscovite mica, Phys. Rev. Lett. 67 (19) (1991) 2642–2645.
[5] A. Erdemir, J.M. Martin, Superlubricity, Elsevier, 2007.
[6] E. Meyer, E. Gnecco, Superlubricity on the nanometer scale, Friction 2 (2) (2014) 106–113.
[7] M.Z. Baykara, M.R. Vazirisereshk, A. Martini, Emerging superlubricity: a review of the state of the art and perspectives on future research, Appl. Phys. Rev. 5 (4) (2018), 041102.
[8] D. Berman, A. Erdemir, A.V. Sumant, Approaches for achieving superlubricity in two dimensional materials, ACS Nano 12 (3) (2018) 2122–2137.
[9] D. Berman, S.A. Deshmukh, S.K.R.S. Sankaranarayanan, A. Erdemir, A.V. Sumant, Macroscale superlubricity enabled by graphene nanoscroll formation, Science 348 (6239) (2015) 1118–1122.
[10] J.M. Martin, C. Donnet, T.h. Le Mogne, T.h. Epicier, Superlubricity of molybdenum disulphide, Phys. Rev. B 48 (14) (1993) 10583–10586.
[11] H. Li, J. Wang, S. Gao, Q. Chen, L. Peng, K. Liu, X. Wei, Superlubricity between MoS_2 monolayers, Adv. Mater. 29 (2017) 1701474.
[12] O. Hod, E. Meyer, Q. Zheng, M. Urbakh, Structural superlubricity and ultralow friction across the length scales, Nature 563 (2018) 485–492.
[13] S. Zhang, T. Ma, A. Erdemir, Q. Li, Tribology of two-dimensional materials: from mechanisms to modulating strategies, Mater. Today 26 (2019) 67–86.
[14] Z. Liu, J. Yang, F. Grey, J.Z. Liu, Y. Liu, Y. Wang, Y. Yang, Y. Cheng, Q. Zheng, Observation of microscale superlubricity in graphite, Phys. Rev. Lett. 108 (20) (2012), 205503.
[15] Y. Song, D. Mandelli, O. Hod, M. Urbakh, M. Ma, Q. Zheng, Robust microscale superlubricity in graphite/hexagonal boron nitride layered heterojunctions, Nat. Mater. 17 (2018) 894–899.
[16] S.W. Liu, H.P. Wang, Q. Xu, T.B. Ma, G. Yu, C. Zhang, D. Geng, Z. Yu, S. Zhang, W. Wang, Y.Z. Hu, H. Wang, J. Luo, Robust microscale superlubricity under high contact pressure enabled by graphene-coated microsphere, Nat. Commun. 8 (2017) 14029.
[17] B. Vasić, A. Matković, R. Gajić, I. Stanković, Wear properties of graphene edges probed by atomic force microscopy based lateral manipulation, Carbon 107 (2016) 723–732.
[18] Y, Qi, J, Liu, Y, Dong, X, Feng, Q, Li, Impacts of environments on nanoscale wear behavior of graphene: Edge passivation vs. substrate pinning. Carbon, 2018, 139: 59–66.
[19] Y. Huang, Q. Yao, Y. Qi, Y. Cheng, H. Wang, Q. Li, Y. Meng, Wear evolution of monolayer graphene at the macroscale, Carbon 115 (2017) 600–607.
[20] X. Li, D. Zhang, X. Xu, K.R. Lee, Tailoring the nanostructure of graphene as an oil-based additive: toward synergistic lubrication with an amorphous carbon film, ACS Appl. Mater. Interfaces 12 (38) (2020) 43320–43330.
[21] X. Li, X. Xu, J. Qi, D. Zhang, A. Wang, K.R. Lee, Insights into superlow friction and instability of hydrogenated amorphous carbon/fluid nanocomposite interface, ACS Appl. Mater. Interfaces 13 (29) (2021) 35173–35186.
[22] X. Liu, J. Yang, J. Hao, J. Zheng, Q. Gong, W. Liu, A near-frictionless and extremely elastic hydrogenated amorphous carbon film with self-assembled dual nanostructure, Adv. Mater. 24 (2012) 4614–4617.
[23] L. Wei, B. Zhang, Y. Zhou, L. Qiang, J. Zhang, Ultra-low friction of fluorine-doped hydrogenated carbon film with curved graphitic structure, Surf. Interface Anal. 45 (8) (2013) 1233–1237.
[24] X. Chen, T. Kato, M. Nosaka, Origin of superlubricity in a-C:H: Si films: a relation to film bonding structure and environmental molecular characteristic, ACS Appl. Mater. Interfaces 6 (16) (2014) 13389–13405.
[25] K. Bewilogua, D. Hofmann, History of diamond-like carbon films — from first experiments to worldwide applications, Surf. Coat. Technol. 242 (2014) 214–225.
[26] J. Robertson, Diamond-like amorphous carbon, Mat. Sci. Eng. R 37 (2002) 129–281.
[27] X. Chen, C. Zhang, T. Kato, X. Yang, S. Wu, R. Wang, M. Nosaka, J. Luo, Evolution of tribo-induced interfacial nanostructures governing superlubricity in a-C: H and a-C:H: Si films, Nat. Commun. 8 (2017) 1675.
[28] T.B. Ma, Y.Z. Hu, H. Wang, Molecular dynamics simulation of shear-induced graphitization of amorphous carbon films, Carbon 47 (2009) 1953–1957.
[29] X. Li, A. Wang, K.R. Lee, Fundamental understanding on low-friction mechanisms at amorphous carbon interface from reactive molecular dynamics simulation, Carbon 170 (2020) 621–629.
[30] A. Erdemir, The role of hydrogen in tribological properties of diamond-like carbon films, Surf. Coat. Technol. 146–147 (2001) 292–297.
[31] X. Li, A. Wang, K.R. Lee, Atomistic understanding on friction behavior of amorphous carbon films induced by surface hydrogenated modification, Tribol. Int. 136 (2019) 446–454.
[32] P. Wu, X. Li, C. Zhang, X. Chen, S. Lin, H. Sun, C.T. Lin, H. Zhu, J. Luo, Self-assembled graphene film as low friction solid lubricant in macroscale contact, ACS Appl. Mater. Interfaces 9 (2017) 21554–21562.
[33] S. Plimpton, Fast parallel algorithms for short-range molecular dynamics, J. Comp. Phys. 117 (1995) 1–19.
[34] S.G. Srinivasan, A.C.T. Van Duin, P. Ganesh, Development of a ReaxFF potential for carbon condensed phases and its application to the thermal fragmentation of a large fullerene, J. Phys. Chem. A 119 (2015) 571–580.
[35] X. Li, H. Mizuseki, S.J. Pai, K.R. Lee, Reactive molecular dynamics simulation of the amorphous carbon growth: effect of the carbon triple bonds, Comput. Mater. Sci. 169 (2019), 109143.
[36] F. Tavazza, T.P. Senftle, C. Zou, C.A. Becker, A.C.T. Van Duin, Molecular dynamics investigation of the effects of tip-substrate interactions during nanoindentation, J. Phys. Chem. C 119 (2015) 13580–13589.
[37] X. Li, A. Wang, K.R. Lee, Mechanism of contact pressure-induced friction at the amorphous carbon/alpha olefin interface, npj Comput. Mater. 4 (2018) 53.
[38] S.J. Stuart, A.B. Tutein, J.A. Harrison, A reactive potential for hydrocarbons with intermolecular interactions, J. Chem. Phys. 112 (14) (2000) 6472–6486.
[39] X. Li, A. Wang, K.R. Lee, Comparison of empirical potentials for calculating structural properties of amorphous carbon films by molecular dynamics simulation, Comput. Mater. Sci. 151 (2018) 246–254.
[40] D.J. Evans, B.L. Holian, The nose-hoover thermostat, J. Chem. Phys. 83 (1985) 4069–4074.
[41] G.T. Gao, P.T. Mikulskl, J.A. Harrison, Molecular-scale tribology of amorphous carbon coatings: effect of film thickness, adhesion, and long-range interactions, J. Am. Chem. Soc. 124 (2002) 7202–7209.
[42] H.J.C. Berendsen, J.P.M. Postma, W.F. van Gunsteren, A. DiNola, J.R. Haak, Molecular dynamics with coupling to an external bath, J. Chem. Phys. 81 (1984) 3684–3690.
[43] X. Li, A. Wang, K.R. Lee, Tribo-induced structural transformation and lubricant dissociation at amorphous carbon-alpha olefin interface, Adv. Theory Simul. 2 (2019) 1800157.
[44] T. Kuwahara, P.A. Romero, S. Makowski, V. Weihnacht, G. Moras, M. Moseler, Mechano-chemical decomposition of organic friction modifiers with multiple reactive centers induces superlubricity of ta-C, Nat. Commun. 10 (2019) 151.
[45] S. Bai, H. Murabayashi, Y. Kobayashi, Y. Higuchi, N. Ozawa, K. Adachi, J. Martin, M. Kubo, Tight-binding quantum chemical molecular dynamics simulations of the low friction mechanism of fluorine-terminated diamond-like carbon films, RSC Adv. 4 (2014) 33739–33748.
[46] L. Cui, Z. Lu, L. Wang, Probing the low-friction mechanism of diamond-like carbon by varying of sliding velocity and vacuum pressure, Carbon 66 (2014) 259–266.

[47] X. Li, A. Wang, K.R. Lee, Insights on low-friction mechanism of amorphous carbon films from reactive molecular dynamics study, Tribol. Int. 131 (2019) 567–578.
[48] S.H. Choi, S.J. Yun, Y.S. Won, C.S. Oh, S.M. Kim, K.K. Kim, Y.H. Lee, Large-scale synthesis of graphene and other 2D materials towards industrialization, Nat. Commun. 13 (2022) 1484.
[49] Y. Peng, W. Zhao, F. Ni, W. Yu, X. Liu, Forest-like laser-induced graphene film with ultrahigh solar energy utilization efficiency, ACS Nano 15 (2021) 19490–19502.